

# Nanoscale

Accepted Manuscript



This is an *Accepted Manuscript*, which has been through the Royal Society of Chemistry peer review process and has been accepted for publication.

*Accepted Manuscripts* are published online shortly after acceptance, before technical editing, formatting and proof reading. Using this free service, authors can make their results available to the community, in citable form, before we publish the edited article. We will replace this *Accepted Manuscript* with the edited and formatted *Advance Article* as soon as it is available.

You can find more information about *Accepted Manuscripts* in the [Information for Authors](#).

Please note that technical editing may introduce minor changes to the text and/or graphics, which may alter content. The journal's standard [Terms & Conditions](#) and the [Ethical guidelines](#) still apply. In no event shall the Royal Society of Chemistry be held responsible for any errors or omissions in this *Accepted Manuscript* or any consequences arising from the use of any information it contains.

## ARTICLE

# Insights into Surface Properties of Oxides on Catalytic Activity of Pd for C—C Coupling Reactions

Cite this: DOI: 10.1039/x0xx00000x

Sai Zhang,<sup>a</sup> Jing Li,<sup>a</sup> Wei Gao,<sup>a</sup> and Yongquan Qu<sup>\*a,b</sup>

Received 00th January 2012,

Accepted 00th January 2012

DOI: 10.1039/x0xx00000x

www.rsc.org/

Understanding interaction between Pd nanocatalysts and metal oxide supports for heterogeneous C-C coupling reactions is still ambiguous since many factors influence the catalytic behavior of Pd nanocatalysts. Herein, three porous nanorods of CeO<sub>2</sub> with controllable surface properties were employed as supports for Pd nanocatalysts with similar dispersion, which avoided the impact of other factors including surface area, morphology and accessible active sites. It provides an ideal approach to probe synergetic catalytic behavior of metal nanoparticles on supports. By studying three C-C coupling reactions (Ullman, Suzuki and Heck), results indicate a strong correlation between the surface properties of supports and catalytic activity of Pd nanocatalysts: supports with a strong basicity and a high concentration of oxygen vacancies result in a rich electron density of Pd and accelerate the first step of oxidative addition reaction for C-C coupling. Infrared spectroscopic study on  $\nu[\text{CO}]$  of CO-treated catalysts and XPS analysis of Pd(3d) core level provide strong evidence supporting in the interaction of Pd/supports for C-C coupling reactions.

## Introduction

The fabrication of multicomponent composite catalysts to achieve more satisfactory catalytic performance has been emerging as an effective approach for designing novel heterogeneous catalysts with high catalytic efficiency.<sup>1-5</sup> Carbon-carbon (C-C) cross-coupling reactions are among the most useful and widely studied in recent decades, for example, in the production of agrochemical and pharmaceutical drugs or in material science.<sup>6,7</sup> With the advantages of repeatable use of catalysts, easy separation of catalysts from products, *etc.*, the immobilization of Pd nanocatalysts on common substrates (such as carbon, silica, alumina or zeolites), has been developed to yield the high efficient catalysis for C-C coupling reactions.<sup>8-14</sup> Generally, these substrates are introduced mainly to prevent nanoparticles from agglomeration or benefit recycling of catalysts. Meanwhile, the surface properties of supports may have an great influence on catalytic activity of Pd nanocatalysts. A recent study indicated the improved activity of Pd/NiFe<sub>2</sub>O<sub>4</sub> for Suzuki and Heck C-C coupling reactions originated from basicity of supports.<sup>15</sup> However, no experimental evidence has verified that. Understanding of the interfacial effect between metal/support is still unclear for C-C coupling reactions since many factors influence catalytic behavior of Pd nanocatalysts, such as the accessible Pd active sites, surface area and morphology of supports and physicochemical properties of supports.

Ceria as an electron acceptor can chemisorb pyrrole or CO<sub>2</sub>, which is a characteristic of Lewis basic sites.<sup>16-18</sup> Recently, we reported a novel nanostructure — porous nanorods of ceria (*PN-CeO<sub>2</sub>*) with a large surface area, a high surface Ce<sup>3+</sup> fraction associated with a high concentration of oxygen vacancies and a strong basicity, which delivered a high catalytic activity towards CO oxidation.<sup>19</sup> The physicochemical properties of *PN-CeO<sub>2</sub>* indicate a strong metal-support interaction (SMSI), which is very critical for many organic reactions.<sup>20</sup> Herein, we demonstrate the surface properties of *PN-CeO<sub>2</sub>* can be regulated by different hydrothermal temperatures, while the similar surface area and same morphology of *PN-CeO<sub>2</sub>* are preserved. Pd displays almost same dispersion at *PN-CeO<sub>2</sub>* treated at different temperatures. Hence, it delivers an intuitionistic platform to illustrate an unambiguous relationship between surface properties of supports and Pd for C-C coupling reactions, in which *PN-CeO<sub>2</sub>* treated at different temperatures were employed as the supports and other factors on catalytic activity of Pd can be effectively avoided. Results indicate that the supports with strong basicity and high concentration of oxygen vacancies lead to rich electron density of Pd and accelerate the first step of oxidative addition for C-C coupling reactions. Infrared spectroscopic studies on  $\nu[\text{CO}]$  of CO-treated catalysts and XPS analysis of Pd(3d) core level further provide the direct experimental evidence for the interaction between Pd nanocatalysts and *PN-CeO<sub>2</sub>* supports.

## Results and Discussion

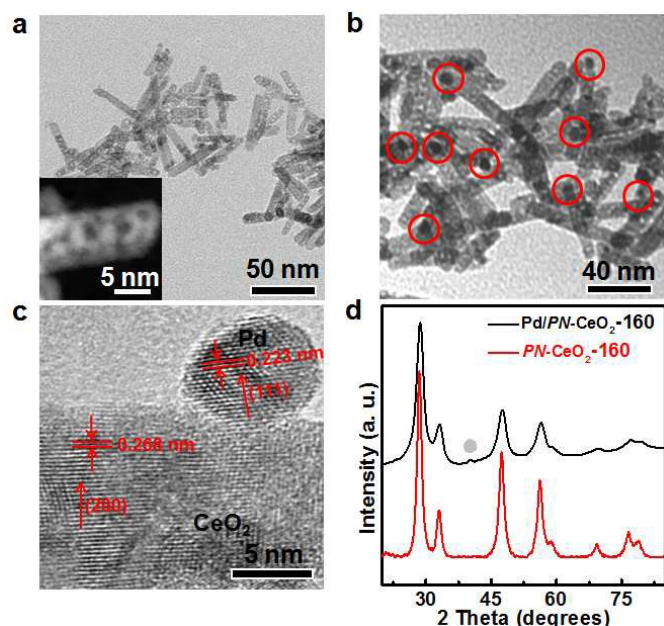


**Fig. 1** (a) Bright field TEM. The inset image is a dark field TEM image of  $PN-CeO_2-160$ . (b) TEM image of  $Pd/PN-CeO_2-160$ . Pd nanoparticles are marked with red circles. (c) HRTEM image of  $Pd/PN-CeO_2-160$ . (d) XRD patterns of  $PN-CeO_2-160$  and  $Pd/PN-CeO_2-160$ . Gray circle represents diffraction peak of Pd nanoparticles.

The synthetic method and characterization of  $PN-CeO_2$  have been reported previously.<sup>19</sup> The  $CeO_2/Ce(OH)_3$  nanorods as the precursor were obtained in the first hydrothermal treatment at 100 °C and the formation of porous  $CeO_2$  nanorods were occurred at the second hydrothermal dehydration at 160 °C. The obtained porous  $CeO_2$  nanorods were named as  $PN-CeO_2-160$ . Transmission electron microscopy (TEM) is used to determine the morphology of as-synthesized nanostructures. From the TEM image of  $PN-CeO_2-160$  (Fig. 1a), the nanocrystals show a rod-like morphology with the diameter of ~ 6 nm and the length of ~ 50 nm; and the porous structure is clearly observed from the dark field TEM image (Inset image, Fig. 1a). This porous structure increases the specific surface area and allows more active site to be exposed, which will facilitate the improvement of the catalytic activity. The X-ray diffraction (XRD) pattern for  $PN-CeO_2-160$  is presented in Fig. 1d. It can be seen that the  $PN-CeO_2-160$  have a well crystal structure. Peaks observed at  $2\theta=28.6, 33.1, 47.4, 56.2, 58.8, 69.2$  and  $76.5^\circ$  are attributed to the (111), (200), (220), (311), (222), (400) and (311) reflections of cubic fluorite  $CeO_2$  (PDF # 34-0394).

$Pd/PN-CeO_2-160$  catalysts with a 3 wt% metal loading were prepared by a modified deposition-precipitation method.<sup>21, 22</sup> As shown in Fig. 1b, Pd nanoparticles are deposited on the surface of  $PN-CeO_2-160$  without any destruction of the porous structure during preparation process. The diameter of Pd nanoparticles is ~ 4.5 nm, which has been verified to exhibit a good catalytic activity for C-C coupling reactions.<sup>23, 24</sup> The clear lattice fringes in the HRTEM image of  $Pd/PN-160-CeO_2$

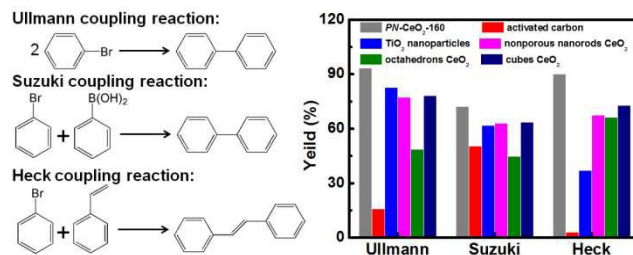


**Fig. 2** The GC yield of C-C coupling reactions for Pd nanoparticles catalysts on different supports. **Reaction conditions of Ullmann coupling reaction:** bromobenzene (0.5 mmol), glucose (100 mg),  $Et_3N$  (1.5 mmol) and catalysts (5 mg),  $H_2O$  (4 mL), 90 °C and 4 h. **Reaction conditions of Suzuki reaction:** bromobenzene (0.5 mmol), phenylboronic acid (0.6 mmol),  $K_2CO_3$  (1.5 mmol) and catalytic (5 mg), 4 mL of solvent,  $V(DMF:H_2O)$  of 1:1, 90 °C and 1 h. **Reaction conditions of Heck coupling reaction:** bromobenzene (0.5 mmol), styrene (0.6 mmol),  $K_2CO_3$  (1.5 mmol) and catalytic (5 mg), 4 mL of solvent,  $V(DMF:H_2O)$  of 1:1, 120 °C and 14 h.

exhibit a good crystallinity of the as-prepared Pd nanoparticles and  $CeO_2$  nanorods (Fig. 1c). The measured planar spacing of 0.223 nm for Pd nanoparticles and 0.268 nm for  $CeO_2$  nanorods are in good agreement with the (111) crystalline plane of Pd and (200) crystalline of cubic fluorite  $CeO_2$ , respectively. A small peak of XRD spectrum at  $2\theta=40.2^\circ$  (Fig. 1d) is attributable to the (111) reflection of Pd, which also proves successful loading of Pd catalysts on  $PN-CeO_2-160$ .

To explore the catalytic activity of  $Pd/PN-CeO_2-160$  catalysts and investigate interface between Pd nanocatalysts and supports, the Ullmann, Suzuki and Heck C-C coupling reactions were performed. The optimization of reaction conditions for the three coupling reactions was shown in Table S1, S2 and S3. At the optimized reaction condition, the kinetic studies of  $Pd/PN-160-CeO_2$  catalytic reactions were also investigated and shown in Fig. S1 (ESI†). The conversion of the reactants was continuously increased with the increase of reaction time. As a comparison, under the optimum conditions, a variety of supports including activated carbon,  $TiO_2$  and nonporous nanorods  $CeO_2$ , cubes  $CeO_2$  and octahedrons  $CeO_2$  were also used as the supports for Pd nanocatalysts immobilization by the same deposition-precipitation method in order to get an impression on the influence of surface properties of various supports. Pd nanocatalysts on various supports displayed similar size of 3.5-6.5 nm (Fig. S2-S6, ESI†). The Pd loading was controlled at 3 wt% for all catalysts.

The catalytic activity of Pd nanocatalysts on different supports for C-C coupling reactions is shown in Fig. 2 and listed in Table S4 with an order:  $PN-CeO_2-160 > TiO_2 > activated carbon$ . Taking the Ullmann coupling reaction of bromobenzene as an example, the GC yield is 93.4% for  $Pd/PN-CeO_2-160$ , in comparison to 82.7% with  $Pd/TiO_2$ , and only 16.0% with  $Pd/C$ . The trend of catalytic activity of Pd nanocatalysts on the different ceria nano-structures is also drawn, with the descending order of  $PN-CeO_2-160$ , followed by cubes  $CeO_2$  and nonporous nanorods  $CeO_2$ , and the lowest conversion of reactants for octahedrons  $CeO_2$ . Still taking an example of Ullmann coupling reaction, the yield is 93.4% for

Pd/*PN*-CeO<sub>2</sub>-160, in comparison to 78.2% with Pd/cubes CeO<sub>2</sub> and 77.2% with Pd/nonporous nanorods CeO<sub>2</sub>, and only 48.8% with Pd/octahedrons CeO<sub>2</sub>. It clearly indicated that the type of catalyst supports plays an important role in determining their catalytic activity. The Pd nanocatalysts on *PN*-CeO<sub>2</sub>-160 showed remarkably higher catalytic activity than those on other common supports for Ullmann reaction, which was also observed for Suzuki (between bromobenzene and phenylboronic acid) and Heck (between bromobenzene and styrene) coupling reactions. The high catalytic activity of *PN*-CeO<sub>2</sub>-160 may be ascribed to a synergistically catalytic effect between Pd nanocatalysts and *PN*-CeO<sub>2</sub>-160 supports. Previous studies simply attributed such similar observations to the basicity of supports.<sup>15, 25-27</sup> However, it is obscure to explain catalytic activity of Pd on supports by their basicity since many factors affect catalytic behavior of Pd for C-C coupling reactions, such as their different surface areas, morphologies, crystal surfaces, metal dispersion, material synthesis method, *et al.*

Before solving this problem, the mechanism of Pd catalyzed C-C coupling is surveyed. Although there have been different views in the literatures on the homogeneous or heterogeneous catalytic mechanisms of Pd catalysts for the C-C coupling reactions, the oxidative addition reaction, the formation of the intermediates ArPd<sup>II</sup>X, is regarded as the key step.<sup>2, 28</sup> The activated or electron enriched Pd nanoparticles can be more easily oxidized into Pd(II) than unactivated Pd nanoparticles by reactant Ar-X at the surface of heterogeneous catalyst. Apparently, the choice of proper supports may enrich electron density of Pd and improve its catalytic activity. Ceria belongs to the fluorite structure, in which each O<sup>2-</sup> anion is surrounded by a tetrahedron of Ce<sup>4+</sup> cations located at the centre of a cubic arrangement of equivalent O<sup>2-</sup> atoms. Non-stoichiometric oxides CeO<sub>2-x</sub>, obtained through wet-chemical synthesis, have a high concentration of oxygen vacancies associated high density of Lewis-base sites. The high catalytic activity of Pd on *PN*-CeO<sub>2</sub> can be ascribed to their surface properties, which easily activate the Pd to reach the highest catalytic activity for C-C coupling reactions by electron donating from supports. However, it is still difficult to understand the interaction between Pd nanocatalysts and supports due to the multiple factors for C-C coupling reactions. To truly understand the surface properties of supports in promoting the catalytic activity of Pd, series of *PN*-CeO<sub>2</sub> with similar morphology and surface areas but different surface properties, synthesized by hydrothermal dehydration on CeO<sub>2</sub>/Ce(OH)<sub>3</sub> nanorods precursor at 180 °C and 200 °C (denoted as *PN*-CeO<sub>2</sub>-180 and *PN*-CeO<sub>2</sub>-200, respectively), provide an ideal platform to study synergistic interaction between the supports and Pd nanocatalysts for C-C coupling reaction.

As shown in Fig. S6 and S7 (ESI<sup>†</sup>), as-synthesized nanostructure treated at 180 °C and 200 °C displayed the porous feature, similar to *PN*-CeO<sub>2</sub>-160. The porous nanorods reached similar surface areas of 141, 131 and 122 m<sup>2</sup>/g for supports synthesized at 160 °C, 180 °C and 200 °C,

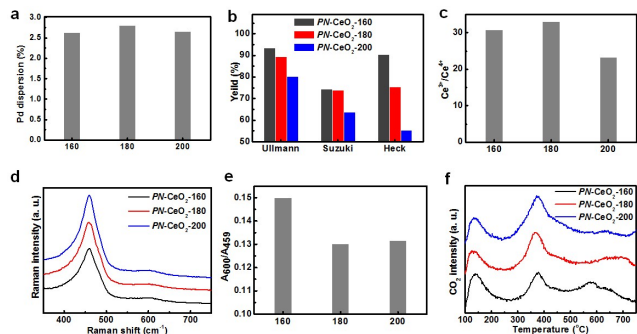


**Fig. 3** (a) Pd dispersion on *PN*-CeO<sub>2</sub> supports. (b) Catalytic activity test of Pd/*PN*-CeO<sub>2</sub> catalysts for three C-C coupling reactions. (c) Surface Ce<sup>3+</sup> fractions of *PN*-CeO<sub>2</sub> supports. (d) Raman spectra of *PN*-CeO<sub>2</sub> supports. (e) Ratio of the integrated peak areas under the bands at 600 and 459 cm<sup>-1</sup> of *PN*-CeO<sub>2</sub> supports. (f) CO<sub>2</sub>-TPD profiles of *PN*-CeO<sub>2</sub> supports.

respectively. Therefore, such series of the *PN*-CeO<sub>2</sub> employed as the supports can avoid the interference factors from supports such as synthetic methods, crystal surfaces, surface area, *et al.* TEM results (Fig. S7 and S8, ESI<sup>†</sup>) revealed the Pd size of ~ 4.5 nm on both *PN*-CeO<sub>2</sub>-180 and -200 supports, same to that on *PN*-CeO<sub>2</sub>-160. Further CO chemisorption experiments showed the near identical dispersion of Pd species on three porous nanorods (Fig. 3a), indicating the equivalent accessible catalytic sites for three catalysts. Hence, such a catalytic system provides an opportunity to study the interaction between supports and catalytic performance of Pd for C-C coupling reactions.

The catalytic activity of Pd/*PN*-CeO<sub>2</sub> for C-C coupling reactions was summarized in Fig. 3b and Table S5. For three C-C coupling reactions, the catalytic activity exhibits the same trend for different porous CeO<sub>2</sub> nanorods. Regarding to the hydrothermal temperatures, the Pd/*PN*-CeO<sub>2</sub>-160 catalysts demonstrated the highest catalytic activity in terms of the highest values of GC yield. Especially for Heck reaction, the GC yield of 90.3 % catalyzed by Pd/*PN*-CeO<sub>2</sub>-160, which was 1.20 and 1.63 times higher than those by Pd/*PN*-CeO<sub>2</sub>-180 (75.4 %) and Pd/*PN*-CeO<sub>2</sub>-200 (55.3 %), respectively. If normalizing to the Pd dispersion, the enhancement factors of catalytic activity of Pd/*PN*-CeO<sub>2</sub>-160 over Pd/*PN*-CeO<sub>2</sub>-180 and Pd/*PN*-CeO<sub>2</sub>-200 were 1.28 and 1.65, respectively. Their catalytic activity was undoubtedly ascribed to the physicochemical properties of three porous nanorods. The surface properties of *PN*-CeO<sub>2</sub>, including surface Ce<sup>3+</sup> fraction and oxygen vacancies concentration and surface basicity, are presented in Fig. 3c, d and e, which reveal a strong correlation to their hydrothermal dehydration temperatures.

The partial elimination of oxygen atoms from O<sup>2-</sup> in the ceria structure forms O-vacancy. The remaining electrons may be a priori either completely delocalized in the conductor band, or distributed among few Ce<sup>3+</sup> cations surrounding the O-vacancy, or localized on Ce<sup>4+</sup> to form Ce<sup>3+</sup>.<sup>29, 30</sup> Therefore, the surface Ce<sup>3+</sup> is rich of electron and tends to provide electrons to metal catalysts.<sup>31</sup> Meanwhile, water dissociation has been examined on the O-vacancy and the dissociation of water gives the reactive OH adspecies.<sup>32</sup>

Both surface  $\text{Ce}^{3+}$  species and OH adspecies are reactive  $\delta^-$  sites, which can donate electrons to Pd deposited on *PN*-CeO<sub>2</sub> supports. Therefore, the surface basicity of *PN*-CeO<sub>2</sub> has a strong correlation with surface  $\text{Ce}^{3+}$  fraction and O-vacancy concentration. They can be used to understand the synergistically catalytic effect for improved the catalytic activity in C-C coupling reactions.

Fig. 3c presents the  $\text{Ce}^{3+}$  fractions of *PN*-CeO<sub>2</sub> treated at different temperatures calculated from their X-ray photoelectron (XPS) spectra (Fig. S9, ESI†). The surface  $\text{Ce}^{3+}$  fractions were 30.8%, 33.0% and 23.3% for *PN*-CeO<sub>2</sub>-160, -180 and -200, respectively. Raman spectroscopy was employed to evaluate the concentration of oxygen vacancies of supports as shown in Fig. 3d. The main peak at 459 cm<sup>-1</sup> is ascribed to the symmetrical stretching mode of the fluorite crystal unit. The peak at 600 cm<sup>-1</sup> indicates the presence of oxygen vacancies in the ceria lattice. The ratio of the integral peak areas at 600 and 459 cm<sup>-1</sup> ( $A_{600}/A_{459}$ ) can be used to quantify the relative concentration of O-vacancy.<sup>33, 34</sup> As shown in the Fig. 3e, the *PN*-CeO<sub>2</sub>-160 also has the highest  $A_{600}/A_{459}$  value of 0.15, which indicates its highest concentration of O-vacancy.

Both surface  $\text{Ce}^{3+}$  fraction and O-vacancy concentration reflect the surface basicity in an order of *PN*-CeO<sub>2</sub>-160 > *PN*-CeO<sub>2</sub>-180 > *PN*-CeO<sub>2</sub>-200. The basicity of supports was also measured by temperature programmed desorption (TPD) with CO<sub>2</sub> as the probe molecule. The CO<sub>2</sub>-TPD peaks representing the base strength distribution of *PN*-CeO<sub>2</sub>-160, -180 and -200 are demonstrated in Fig. 3f. The number of weak, medium and strong basic sites can be estimated from the integral area under their TPD curves for the temperature range of 100-250 °C, 250-516 °C and >516 °C, respectively.<sup>35</sup> As calculated results in Table 1 (after normalization of integral area), *PN*-CeO<sub>2</sub>-160 gives a larger number of weak basic sites compared to the *PN*-CeO<sub>2</sub>-180 and -200. Meanwhile, it also exhibits an obvious desorption peak in strong basic sites, and the area of strong basic sites is about 1.4 and 2.2 times than those of *PN*-CeO<sub>2</sub>-180 and -200, respectively. Although *PN*-CeO<sub>2</sub>-200 shows higher medium basic sites, *PN*-CeO<sub>2</sub>-160 has the highest number of basic sites pertaining to the total weak, medium and strong basic sites. Therefore, *PN*-CeO<sub>2</sub>-160 shows the highest surface degree of basicity.

**Table 1.** Area of peaks for different porous CeO<sub>2</sub> nanorods by CO<sub>2</sub>-TPD

Support	Area of peaks			Total
	Weak (< 250 °C)	Medium (250-516 °C)	Strong (>516 °C)	
<i>PN</i> -CeO <sub>2</sub> -160	2.0	3.6	2.6	8.2
<i>PN</i> -CeO <sub>2</sub> -180	1	3.3	1.8	6.1
<i>PN</i> -CeO <sub>2</sub> -200	1.1	4.2	1.2	6.5

Due to the high surface  $\text{Ce}^{3+}$  fraction and concentration of O-vacancy and strong basic sites of *PN*-CeO<sub>2</sub>-160, Pd on it showed the highest catalytic activity for C-C coupling reactions. A proposed reaction mechanism is illustrated in Fig. 4. During the hydrothermal dehydration of CeO<sub>2</sub>/Ce(OH)<sub>3</sub> nanorods precursor, surface  $\text{Ce}^{3+}$  and O-vacancy are formed as shown in Fig. 4a. The active OH<sup>δ-</sup> species will be generated by the adsorption and dissociation of water on the O-vacancy sites (Fig. 4b).<sup>36, 37</sup> As shown in Fig. 4c, the  $\text{Ce}^{3+}$  and OH<sup>δ-</sup> are the electron pair donors and the electrons can be transferred

to the Pd nanoparticles, leading to their activation. Under the activation by the basic ceria nanorods via the electron-donating effect, the Pd nanoparticles could have a higher electronic density and accelerate the formation of active radical ligand  $\text{ArPd}^{\text{II}}\text{X}$  (Fig. 4d). It facilitates the first step of oxidative addition reaction, and subsequently promotes the catalytic activity of Pd for C-C coupling reactions.

The infrared spectroscopic data of  $\nu[\text{CO}]$  of catalysts treated with CO at room temperature further provides strong experimental evidence, which predicts the electron density of Pd species on *PN*-CeO<sub>2</sub>. In Fig. 4e, compared with initial Pd/*PN*-CeO<sub>2</sub>-160 and *PN*-CeO<sub>2</sub>-160 treatment with CO, another adsorption peak appears at 1700-1745 cm<sup>-1</sup> for all Pd/*PN*-CeO<sub>2</sub> catalysts after treating with CO. It is attributed to the C-O vibrational frequencies of CO on Pd nanoparticles.<sup>38</sup> Meanwhile, we found the  $\nu[\text{CO}]$  followed an order of *PN*-CeO<sub>2</sub>-160 (1701 cm<sup>-1</sup>) < *PN*-CeO<sub>2</sub>-180 (1722 cm<sup>-1</sup>) < *PN*-CeO<sub>2</sub>-200 (1726 cm<sup>-1</sup>), demonstrating the highest electron density of Pd on *PN*-CeO<sub>2</sub>-160. Hence, for the first time, the interaction between substrate and Pd nanocatalysts was unambiguously demonstrated with strong experimental evidences, expressing that a strong basicity associated with high concentration of O-vacancy of supports enriches electron density of metal catalysts and facilitates the oxidative addition for C-C coupling reaction.

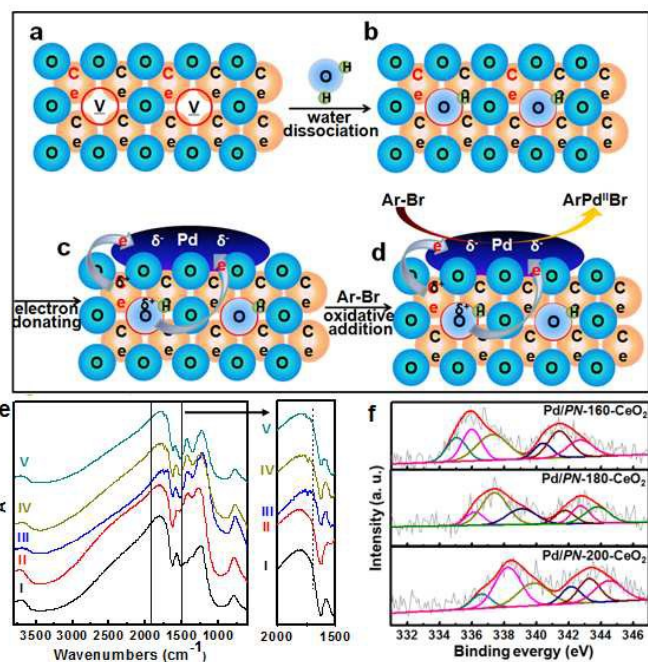


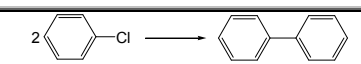
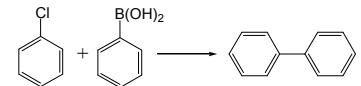
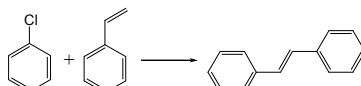
**Fig. 4** (a, b, c and d) The proposed catalytic mechanism for the interaction between *PN*-CeO<sub>2</sub> supports and Pd with improved catalytic activity for C-C coupling reaction. (e) The FT-IR spectra of different catalysis: I is the Pd/*PN*-CeO<sub>2</sub>-160, II, III, IV and V are the *PN*-CeO<sub>2</sub>-160, Pd/*PN*-CeO<sub>2</sub>-160, Pd/*PN*-CeO<sub>2</sub>-180, Pd/*PN*-CeO<sub>2</sub>-200 treatment with CO at room temperature, respectively. (f) The XPS analysis of Pd nanoparticles in different catalysts.

XPS analysis of Pd(3d) core level region of Pd/*PN*-CeO<sub>2</sub> catalysts were shown in Fig. 4f. The binding energy of Pd(3d<sub>5/2</sub>)

increases from 335.8 eV to 337.2 eV and than 338.4 eV for Pd/PN-160-CeO<sub>2</sub>, Pd/PN-180-CeO<sub>2</sub> and Pd/PN-200-CeO<sub>2</sub>, respectively. The binding energy of Pd(3d<sub>3/2</sub>) exhibited the same trend of those of Pd(3d<sub>5/2</sub>). The increased binding energy shows the more oxide phases in which Pd atoms are coordinated to two and four O<sup>2-</sup> neighbours, respectively.<sup>39, 40</sup> Hence, Pd/PN-160-CeO<sub>2</sub> has the least amount of oxidized Pd species, demonstrating the highest electron density of Pd on PN-CeO<sub>2</sub>-160. The results further confirm that Pd nanocatalysts immobilized on the strong basic supports can make the high electric density, which could further facilitate the C-C coupling reactions.

Due to the ready availability and low expense, the use of aryl chlorides is highly desirable from a practical point of view. Although there have been many reports of heterogeneous reactions in the literatures, there are quite rare successful examples using less active aryl chlorides.<sup>41, 42</sup> Because aryl chlorides are much more difficult to be activated than aryl iodides and bromides due to the strong covalent bond of C-Cl, the activation of aryl halides is particularly challenging for heterogeneous catalysts. The Pd/PN-CeO<sub>2</sub>-160 can effectively activate the C-Cl bond and efficiently catalyze C-C coupling reaction using aryl chlorides as resources (Table 2). The Ullmann and Suzuki coupling reactions were initially carried out in 90 °C, while the Heck coupling reaction was performed at 120 °C. With 15 mg Pd/PN-CeO<sub>2</sub>-160 catalysts, the Ullmann and Suzuki coupling reaction can occur completely with a 100% GC yield within 2 h. The Heck coupling reaction gives a yield of 59.6% within 12 h.

**Table 2.** The C-C coupling reactions of aryl chlorine by Pd/PN-CeO<sub>2</sub>-160 \*

Reaction	Time (h)	Yield (%)
	2	100
	2	100
	12	59.6

\* **Reaction conditions:** The reaction conditions are the same as shown in Figure 2 with 15 mg Pd/PN-CeO<sub>2</sub>-160 catalysts, except changing the bromobenzene to chlorobenzene.

The reusability of Pd/PN-160-CeO<sub>2</sub> catalysts for the C-C coupling reactions between bromobenzene and phenylboronic acid were also performed (Fig. S10, ESI†). For 5 cycles, the yield of the Suzuki coupling reaction exhibited a good stability, demonstrating the benefits of the catalysts for the separation and reuse.

## Conclusions

In conclusion, we have experimentally demonstrated the first example exhibiting a strong correlation between the surface properties of the supports and the catalytic activity of Pd

nanocatalysts for C-C coupling reactions. Surface properties of PN-CeO<sub>2</sub> can be controllable by the hydrothermal temperature, while their geometrical feature can be preserved. The other factors including the size and morphology of both supports and Pd nanocatalysts and dispersion of Pd species were excluded by employing the PN-CeO<sub>2</sub> as the support, which provide a straightforward approach to study synergistic interfacial effect between supports and metal catalysts. Our results unambiguously demonstrate that the PN-CeO<sub>2</sub>-160 supports with the high concentration of oxygen vacancies and strong basicity can significantly improve the catalytic activity of metal nanocatalysts for C-C coupling reaction. The infrared spectroscopic studies and XPS analysis provide a direct experimental evidence to confirm that the stronger basicity of the supports can enrich the electron density of loaded Pd nanocatalysts and accelerate the oxidative addition to form ArPd<sup>II</sup>X.

## Acknowledgements

We acknowledge the financial support from a NSFC Grant 21201138. This work was also partially funded by the Ministry of Science and Technology of China through a 973-program under Grant 2012CB619401 and by the Fundamental Research Funds for the Central Universities under Grant xjj2013102 and xjj2013043. Technical supports for TEM from Frontier Institute of Science and Technology. We thank Prof. Pengfei Li for useful discussion.

## Notes and references

<sup>a</sup>Center of Applied Chemical Research, Frontier Institute of Science and Technology, Xi'an Jiaotong University, Xi'an, China 740049. E-mail: yongquan@mail.xjtu.edu.cn.

<sup>b</sup>State Key Laboratory for Mechanical Behavior of Materials, Xi'an Jiaotong University, Xi'an, China, 710049.

† Footnotes should appear here. These might include comments relevant to but not central to the matter under discussion, limited experimental and spectral data, and crystallographic data. Electronic Supplementary Information (ESI) available: [More characterizations of catalysts; calculations of j<sub>0</sub> and TOF]. See DOI: 10.1039/b000000x/

- G. Chen, Y. Zhao, G. Fu, P. N. Duchesne, L. Gu, Y. Zheng, X. Weng, M. Chen, P. Zhang and C.-W. Pao, *Science*, 2014, **344**, 495-499.
- J. Shi, *Chem. Rev.*, 2012, **113**, 2139-2181.
- S. Zander, E. L. Kunkes, M. E. Schuster, J. Schumann, G. Weinberg, D. Teschner, N. Jacobsen, R. Schlögl and M. Behrens, *Angew. Chem. Int. Ed.*, 2013, **52**, 6536-6540.
- X. Huang, Y. Li, Y. Chen, H. Zhou, X. Duan and Y. Huang, *Angew. Chem.*, 2013, **125**, 6179-6183.
- W. Xu, Z. Liu, A. C. Johnston-Peck, S. D. Senanayake, G. Zhou, D. Stacchiola, E. A. Stach and J. A. Rodriguez, *ACS Catal.*, 2013, **3**, 975-984.
- R. Jana, T. P. Pathak and M. S. Sigman, *Chem. Rev.*, 2011, **111**, 1417-1492.
- C. S. Yeung and V. M. Dong, *Chem. Rev.*, 2011, **111**, 1215-1292.
- A. Molnar, *Chem. Rev.*, 2011, **111**, 2251-2320.

- 9 V. Polshettiwar, R. Luque, A. Fihri, H. Zhu, M. Bouhrara and J.-M. Basset, *Chem. Rev.*, 2011, **111**, 3036-3075.
- 10 A. Balanta, C. Godard and C. Claver, *Chem. Soc. Rev.*, 2011, **40**, 4973-4985.
- 11 L. Yin and J. Liebscher, *Chem. Rev.*, 2007, **107**, 133-173.
- 12 M. W. Klaus Köhler, Laurent Djakovitch, *Catal. Today*, 2001, **66**, 114.
- 13 X. Huang, Y. Li, Y. Chen, E. Zhou, Y. Xu, H. Zhou, X. Duan and Y. Huang, *Angew. Chem. Int. Ed.*, 2013, **52**, 2520-2524.
- 14 E. Hariprasad and T. Radhakrishnan, *ACS Catal.*, 2012, **2**, 1179-1186.
- 15 Z. Gao, Y. Feng, F. Cui, Z. Hua, J. Zhou, Y. Zhu and J. Shi, *J. Mol. Catal. A: Chem.*, 2011, **336**, 51-57.
- 16 D. Martin and D. Duprez, *J. Phys. Chem.*, 1996, **100**, 9429-9438.
- 17 K. R. Hahn, M. Iannuzzi, A. P. Seitsonen and J. r. Hutter, *J. Phys. Chem. C*, 2013, **117**, 1701-1711.
- 18 H. Hattori, *Chem. Rev.*, 1995, **95**, 537-558.
- 19 J. Li, Z. Zhang, Z. Tian, X. Zhou, Z. Zheng, Y. Ma and Y. Qu, *J. Mater. Chem. A*, 2014, **2**, 16459-16466.
- 20 A. Bruix, J. A. Rodriguez, P. J. Ramirez, S. D. Senanayake, J. Evans, J. B. Park, D. Stacchiola, P. Liu, J. Hrbek and F. Illas, *J. Am. Chem. Soc.*, 2012, **134**, 8968-8974.
- 21 A. Hugon, L. Delannoy and C. Louis, *Gold Bulletin*, 2008, **41**, 127-138.
- 22 P. Christopher, H. Xin and S. Linic, *Nat. chem.*, 2011, **3**, 467-472.
- 23 Y. Li, E. Boone and M. A. El-Sayed, *Langmuir*, 2002, **18**, 4921-4925.
- 24 M. Crespo-Quesada, A. Yarulin, M. Jin, Y. Xia and L. Kiwi-Minsker, *J. Am. Chem. Soc.*, 2011, **133**, 12787-12794.
- 25 M. L. Kantam, K. B. S. Kumar, P. Srinivas and B. Sreedhar, *Adv. Syn. Catal.*, 2007, **349**, 1141-1149.
- 26 B. Karimi, D. Elhamifar, J. H. Clark and A. J. Hunt, *Chem. Eur. J.*, 2010, **16**, 8047-8053.
- 27 B. Baruwati, D. Guin and S. V. Manorama, *Org. Lett.*, 2007, **9**, 5377-5380.
- 28 J.-P. C. a. G. Mignani, *Chem. Rev.*, 2006, **106**, 2651-2710.
- 29 J. J. Plata, A. M. Márquez and J. F. Sanz, *J. Phys. Chem. C*, 2013, **117**, 25497-25503.
- 30 M. F. Camellone and S. Fabris, *J. Am. Chem. Soc.*, 2009, **131**, 10473-10483.
- 31 H. Y. Kim, H. M. Lee and G. Henkelman, *J. Am. Chem. Soc.*, 2012, **134**, 1560-1570.
- 32 Y.-G. Wang, D. Mei, J. Li and R. Rousseau, *J. Phys. Chem. C*, 2013, **117**, 23082-23089.
- 33 Z.-Y. Pu, J.-Q. Lu, M.-F. Luo and Y.-L. Xie, *J. Phys. Chem. C*, 2007, **111**, 18695-18702.
- 34 M. Guo, J. Lu, Y. Wu, Y. Wang and M. Luo, *Langmuir*, 2011, **27**, 3872-3877.
- 35 N. A. S. A. Istadi and N. A. S. Amin, *J. Mol. Catal. A: Chem*, 2006, **259**, 61-66.
- 36 M. Tamura, A. Satsuma and K.-i. Shimizu, *Catal. Sci. Technol.*, 2013, **3**, 1386-1393.
- 37 Y. Wang, F. Wang, Q. Song, Q. Xin, S. Xu and J. Xu, *J. Am. Chem. Soc.*, 2013, **135**, 1506-1515.
- 38 I. V. Yudanov, R. Sahnoun, K. M. Neyman, N. Rösch, J. Hoffmann, S. Schauer mann, V. Johane k, H. Unterhalt, G. Rupprechter and J. Libuda, *J. Phys. Chem. B*, 2003, **107**, 255-264.
- 39 K. Priolkar, P. Bera, P. Sarode, M. Hegde, S. Emura, R. Kumashiro and N. Lalla, *Chem. Mater.*, 2002, **14**, 2120-2128.
- 40 A. F. Lee, J. N. Naughton, Z. Liu and K. Wilson, *ACS Catal.*, 2012, **2**, 2235-2241.
- 41 M. J. Jin and D. H. Lee, *Angew. Chem.*, 2010, **122**, 1137-1140.
- 42 B. Yuan, Y. Pan, Y. Li, B. Yin and H. Jiang, *Angew. Chem. Int. Ed.*, 2010, **49**, 4054-4058.